Review | Vol. 8, No. 11 | 1 Nov 2018 | OPTICAL MATERIALS EXPRESS 3307
Optical Materials EXPRESS

# Magneto-optical materials and designs for integrated TE- and TM-mode planar waveguide isolators: a review [Invited]

KARTHIK SRINIVASAN* AND BETHANIE J. H. STADLER

*Electrical and Computer Engineering Department, University of Minnesota, Minneapolis, MN 55414, USA*
*srini162@umn.edu

**Abstract:** Optical isolators are unidirectional devices that employ the magneto-optical (MO) property of iron garnets to block the reflected light in almost all optical systems. Sputter deposition of either doped yttrium iron garnets (YIG) with seed-layers or seed-layer free terbium iron garnets (TIG) will help realize integrated planar isolators. Faraday rotation waveguides are designed as a viable solution to enable these monolithically integrated garnets to overcome the limitations inherent to hybrid integration of interferometric devices. In fact, small footprint Faraday rotation devices have been achieved using doped TIG for both TE/TM modes with sufficiently low loss and large isolation ratios.



## 1. Introduction

The ubiquity of high-speed computing and large-scale data storage has resulted in an increase in demand for state-of-the-art technology solutions that are heavily reliant on light as the primary carrier of information [1, 2]. Conventional metallic interconnects on electron-driven platforms will no longer be viable options due to their increasing power requirements resulting from losses due to heat dissipation [3, 4]. Therefore the requirement to minimize the losses and at the same time accommodate increasing computation/communication speed has propelled research in photonic systems resulting in a large number of applications for photonic integrated circuits (PIC) [5–7]. A typical PIC would at the least consist of a light source that drives the rest of the circuitry performing the essential logic/routing functions depending on the site of operation. Since these systems are driven by an on-chip laser, it is of paramount importance to protect these sources from back-reflections that can originate from device interfaces due to the differences in the refractive indices. Isolators are passive devices that can be visualized as the photonic analog of an electronic diode in which a signal propagating in the backward direction can be selectively blocked in the presence of a magnetic field (Fig. 1(a)) [8, 9]. This isolating function can be realized through a monolithically integrated device on a semiconductor platform using magneto-optical materials [10].

Magneto-optical (MO) materials are a unique class of rare-earth iron garnets with an ideal stoichiometry of $R_3Fe_5O_{12}$, which are suitable for realizing non-reciprocal devices. The MO effect in these materials enables the breaking of time reversal symmetry which blocks reflection of light towards the laser [12, 13]. This is because of the non-zero off-diagonal components in the dielectric matrix.

$$\epsilon = \begin{bmatrix} \epsilon_{xx} & 0 & i\epsilon_{xz} \\ 0 & \epsilon_{yy} & 0 \\ -i\epsilon_{xz} & 0 & \epsilon_{zz} \end{bmatrix} \tag{1}$$

$$\epsilon_{xz} = \frac{(n\lambda\theta_F)}{\pi} \tag{2}$$

The diagonal components are the squares of the refractive indices($n_{xx} = n_{yy} = n_{zz} = n$). The

#339880 https://doi.org/10.1364/OME.8.003307
Journal © 2018 Received 16 Jul 2018; revised 18 Sep 2018; accepted 25 Sep 2018; published 10 Oct 2018

Optical Materials EXPRESS

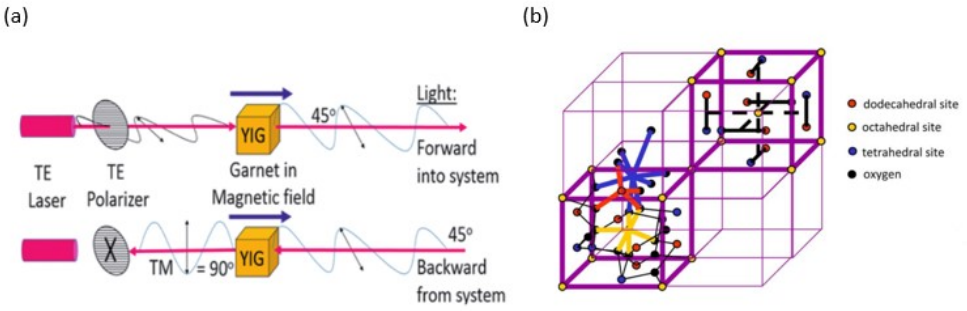


Fig. 1. (a) Graphical representation of an optical isolator based on Faraday rotation. The reflected light is filtered out by a TE mode polarizer, protecting the laser source. Reproduced with permission from [11]. (b) Structure of yttrium iron garnet (YIG) in two representations highlighting the different lattice sites. ©2018 IEEE. Reprinted, with permission, from [10].

off-diagonal component($\epsilon_{xz}$) can be measured and calculated from the Faraday rotation($\theta_F$) and the refractive index of the material at a specific wavelength($\lambda$). Faraday rotation (FR) is a result of the Zeeman splitting that occurs in a resonant transition due to the presence of a magnetic field. Because of this splitting of the absorption peak, there is a divergence between the refractive indices for left- and right-circularly polarized light. This difference is proportional to the FR of the material [14]. However, while evaluating the performance of these MO materials, the associated optical loss also needs to be considered. At the operating wavelengths of 1330nm and 1550nm in the near-infrared regime, yttrium and terbium iron garnets have some of the highest figure-of-merit ($FOM = FR/Loss$) over other alternatives [15, 16]. The lattice structure for an iron garnet is shown in Fig. 1(b), and it should be noted that the MO effect is a result of the arrangement of atoms in specific sites and the net magnetization due its ferrimagnetic alignment. Although there are alternative approaches explored in the past to achieve isolation without using an iron garnet, such techniques were non-passive and required an external power supply making them undesirable [17, 18].

Passive isolators based on MO effects can be categorized as non-reciprocal phase shift (NRPS) or non-reciprocal mode conversion (NMRC) devices, based on their mode of operation. The NRPS devices contain two arms of waveguides in an interferometer or a ring resonator with a garnet top cladding through a vacuum deposition technique like pulsed laser deposition (PLD) or a hybrid integration technique like wafer bonding. In the interferometric NRPS design, a magnetic field is applied transverse to the waveguide arms, and the phase difference between the two waveguide arms results in constructive interference in the forward and destructive interference in the backward directions [19, 20]. However, current NRPS devices are capable of inducing the phase shift only in TM-polarized modes and despite attempts at sidewall coating using PLD, working designs use reciprocal polarization converters (RPC) to enable TE-mode operation [21, 22]. On the other hand, NRMC, which is the waveguide equivalent to Faraday rotation, can be used to realize all-mode isolators [11, 23]. In NRMC devices, the garnet is sputtered as a top cladding on the waveguide, allowing for the propagating mode's evanescent tail to interact with the MO material. A periodically modulated top cladding is employed to obtain quasi-phase matching that overcomes any inherent phase velocity mismatch (birefringence), which is otherwise a limitation to the isolation function of NRMC in waveguides [24]. Both NRPS and NRMC offer excellent alternatives to fiber coupled isolators and provide means of achieving waveguide based integrated isolators for protecting on-chip lasers in PICs.

One of the most important goals in non-reciprocal photonics research is to enable seamless

Optical Materials EXPRESS

monolithic integration with semiconductor platforms using foundry friendly processes. While the success of non-reciprocal devices is attributed to the favorable properties of magneto-optical rare-earth iron garnets, a potential limitation also arises from the difficulty in integration of these materials with silicon substrates. This review can be broadly divided into two parts, magneto-optical materials and non-reciprocal devices. In the materials category, the first section will discuss the initial efforts associated with vacuum deposition of rare-earth iron garnets and the challenges involved with silicon integration. Next, the focus will be shifted towards improving the FOM of the commonly researched growth of the desired phase on non-garnet with advances in improving its phase purity. The final section under materials will discuss the development of other iron garnet systems that have better integration capability with silicon platforms. In the devices section, a brief overview of the NRPS effect and associated devices will be given followed by a thorough discussion on the principle of NRMC and results from the most recent monolithically integrated Faraday rotation waveguide isolators.

## 2. Magneto-optical materials

### 2.1. Sputter deposition of YIG

Conventionally, garnet growth was focused and optimized for epitaxial films, wherein techniques like liquid phase epitaxy (LPE) were used to obtain phase pure single crystal garnet on lattice matched substrates, eg: YIG on gadolinium gallium garnet (GGG) [25]. The potential of metal-organic chemical vapor deposition (MOCVD) as an alternative to LPE for growth of MO material on non-garnet substrates (InP and GaAs) resulted in $0.4°/\mu m$ at $1.3\mu m$ for cerium doped YIG [26]. Despite the initial success, long durations of annealing were not favorable and the efforts were concentrated on identifying a robust process more suited to the needs of semiconductor fabrication technology. The breakthrough came in 2005 when Sung et al. demonstrated the growth of the desired phase YIG on non-garnet substrates using reactive RF magnetron sputtering in partial pressure differential followed by an *ex-situ* rapid thermal annealing (RTA) [27]. The use of Fe and Y metallic targets and short duration RTA under optimized deposition conditions, as shown in the practical phase diagram in Fig. 2(a), resulted in the desired $Y_3Fe_5O_{12}$ phase on both quartz and MgO substrates within a wide processing window. It was observed that upon *ex-situ* RTA of films grown on non-garnet substrates, micro-cracks often formed from the induced strain between the film and the substrate due to a mismatch in coefficient of thermal expansion (CTE). In order to overcome this, the films were patterned into waveguides and annealed [28]. Patterning of the films reduced the effective surface area of the garnet in contact with the substrate thereby reducing the net strain experienced by the film. Sputtered films on $SiO_2/Si$ substrates were masked using photoresist lines of varying widths and etched in $H_3PO_4$ at $43°C$ for several minutes. Figure 2(b) shows that the patterned ridges did not crack and films as thick as $1.5\mu m$ could be sputtered and annealed. Such patterned garnet waveguides can propagate a light of wavelength $1.55\mu m$ with a low loss of 1 dB/mm. This effectively demonstrated the integration of garnet on silicon based platforms, paving way for future research in improving the quality of the material and performance of the device fabricated through monolithic techniques.

### 2.2. Growth optimization of doped garnets

As mentioned earlier, Faraday rotation of a MO material is indicative of the quality of the material and its performance in a non-reciprocal optical device. YIG has an inherently low FR and to improve this one has to think from a materials engineering perspective. Doping became a standard process and it was found that epitaxial cerium doped yttrium iron garnet (Ce:YIG) grown on lattice matched GGG has a FR of $-4500°/cm$ compared to $+200°/cm$ (comparison of absolute values) in undoped YIG (opposite chirality) [29–31]. However, similar attempts to grow

Optical Materials EXPRESS

doped YIG on silicon substrates were unsuccessful due to the mismatch in CTE and formation of secondary phases upon annealing. A new method which introduced an intermediate thin layer (20nm) of undoped garnet on which doped garnet was deposited using PLD demonstrated the first successful growth of desired phase Ce:YIG on Si [32, 33]. Further research was carried out in optimizing the seed layer thickness and reducing the overall thermal budget from the annealing processes. Block et al. demonstrated that sputtering can be used to successfully grow doped garnets with a seed layer and found that the thickness of the seed layer determines the quality of Ce:YIG grown on it [34]. Figure 3(a) shows that for the thinnest seed layer of 7nm, the crystallinity is only 2.9% and close to 100% crystallinity is obtained at 45nm of YIG seed layer. The corresponding XRD in Fig. 3(b) is an indicator of the increasing phase purity of Ce:YIG with seed layers approaching 45nm. Faraday rotation measurements revealed that Ce:YIG grown on a seed layer larger than 45nm in thickness has a rotation of $-3700°/cm$, highest that can be achieved to date through monolithic integration on silicon platforms. Another important aspect in the process of growth and crystallization of YIG/Ce:YIG is the annealing temperature. It has already been mentioned earlier that rapid thermal annealing (RTA) has been adopted as a fast and silicon-compatible technique over annealing in tube furnaces for several hours [27]. But, the RTA temperature required to crystallize YIG can reach up to $900°C$, which may be greater than the allowed thermal budget in the monolithic integration process. Several alternatives have been proposed by other research groups in order to reduce the thermal budget. One such idea is a hybrid integration technique that wafer bonds epitaxial Ce:YIG/GGG onto the device [35]. Another group demonstrated that Ce:YIG can be crystallized on silicon using a top seed layer followed by a single step anneal with desirable FR [36]. *In-situ* crystallization studies in a transmission electron microscope (TEM) revealed that YIG films (25nm) can be fully crystallized with a two-step anneal that has a reduced thermal budget [37]. The *in-situ* annealing was carried out using laser pulses (343 nm, 20-90 mW) at a rate of 25 kHz where the power levels were chosen to mimic a two-step RTA anneal of $400°C$ for 3 min followed by $800°C$ for another 3min. This two-step process reduced the overall thermal budget and improved the crystallinity, similar to *ex-situ* RTA as shown in Fig. 4.

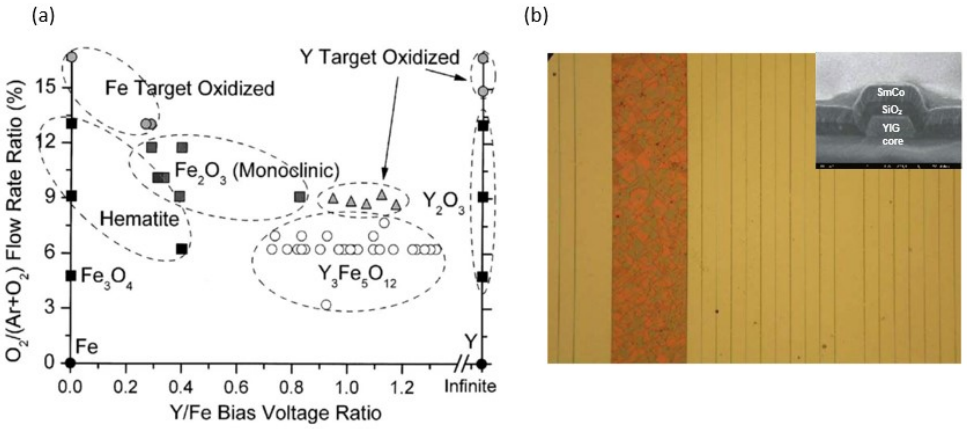


Fig. 2. (a) Phase diagram representing the different phases obtained in sputter deposition of YIG from Fe and Y metallic targets in oxygen. The obtained phases are plotted with respect to their gas flow rate ratio and Y/Fe sputtering bias voltage ratios. Reprinted from [27], with the permission of AIP Publishing. (b) Optical micrograph of patterned $YIG/SiO_2/Si$ waveguides annealed at $700 - 800°C$ for 10-120 s in oxygen. The wide alignment bar ($500\mu m$) cracked on annealing and the inset shows a waveguide without any damage due to high temperature. Reprinted from [28], with the permission of AIP Publishing.

Optical Materials EXPRESS

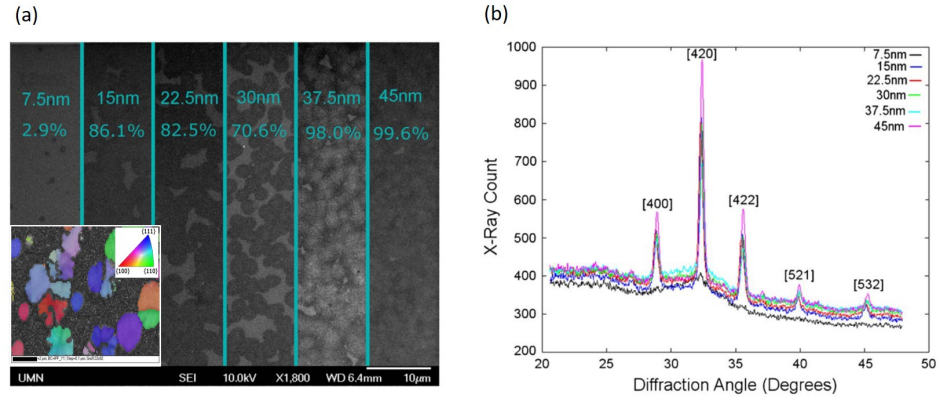


Fig. 3. (a) Scanning electron micrograph of YIG seed layer of varying thicknesses showing a steady increase in crystallinity of the seed layer. The inset is an electron backscatter diffraction (EBSD) image indicative of the film morphology. (b) X-ray diffraction (XRD) spectra of Ce:YIG grown on YIG seed layer of different thicknesses. The 45 nm seed layer gives the best quality Ce:YIG films. ©2018 IEEE. Reprinted, with permission, from [34].

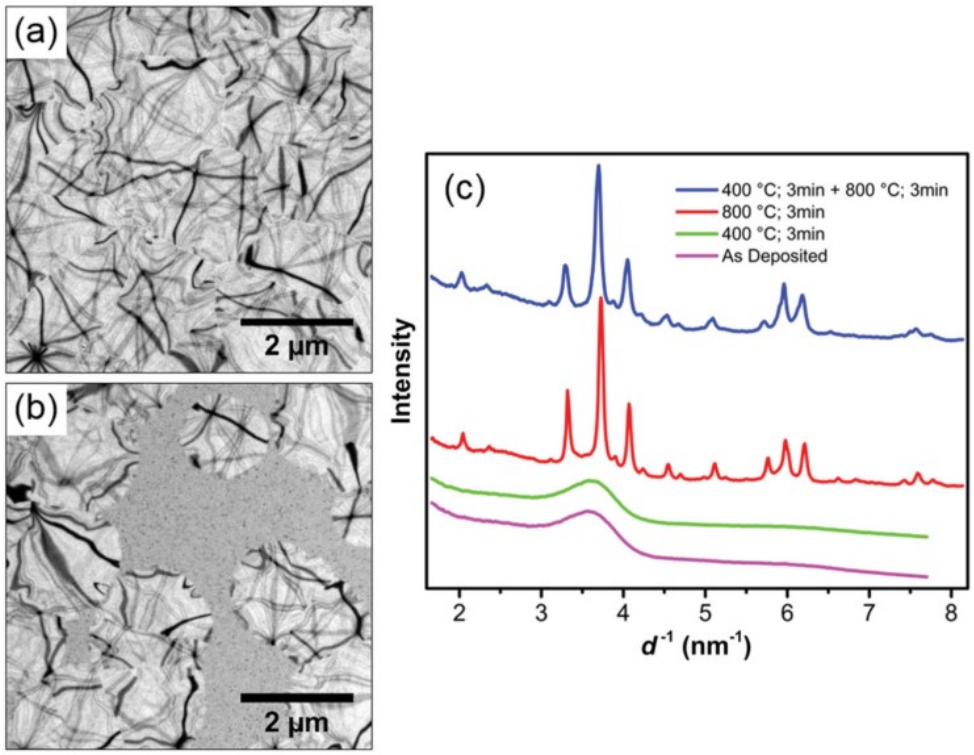


Fig. 4. (a) Bright-field TEM images of 25 nm YIG films on $SiO_2$ (a) annealed at 400°$C$ for 3 min, followed by another anneal at 800°$C$ for 3 min and (b) annealed at 800°$C$ for 3 min in a single step. (c) The radial integration of select area diffraction patterns for films from (a) and (b). The two-step anneal in (a) has produced pure phase YIG in comparison to a single step anneal [37].

Optical Materials EXPRESS

### 2.3. Seed-layer free terbium iron garnets

In spite of the efforts and success in improving the FR of YIG via doping, optimizing the seed layer thickness and reducing the thermal budget, the primary requirement for a seed layer has not been eliminated. Figure 5(a) shows the calculated average $S_3$ Stokes parameter as a function of the thickness of the seed layer for Ce:YIG reported in the literature with different FR coefficients [38]. The $S_3$ Stokes parameter gives the degree of NRMC and/or NRPS, related to the off diagonal element in the dielectric tensor for a TE-like mode. The calculated data is evidence to the fact that the seed layer reduces the interaction of light with the garnet cladding on SOI devices and results in smaller $S_3$ values. In addition to that, it has to be noted that YIG seed layers are not optically dead but rather have a FR contribution of $+200°/cm$. The opposite chirality of the seed layer is detrimental for garnet cladding as the effective FR experienced by the evanescent tail of the propagating mode decreases. Alternative solutions like a top seed layer, while creative indeed, did not demonstrate significant improvements in performance and different seed layer materials could not match the high FR obtained from the Ce:YIG/YIG combination [36].

Garnet core devices were explored as a promising alternative where the light propagates inside the MO material, thereby enabling complete isolation with very short path lengths. It was demonstrated that a quasi-phase matched push-pull garnet waveguide with alternate segments of terbium iron garnet (TIG) and Ce:YIG having FR of $+500°/cm$ and $-3700°/cm$ respectively could achieve a rotation of 45° in $360\mu m$ (Fig. 5(b)) [38]. However, development in PIC technology has largely focused on silicon photonics with light propagation in Si-only cores as an industry compatible standard. Further, a system with garnet core waveguides for isolators can result in reflections at dissimilar interfaces due to difference in the refractive indices ($n^2_{Si} = 11.7$ and $n^2_{YIG} = 4.41$). Therefore, it is safe to conclude that garnet clad SOI devices are the desired designs for photonic isolators. But realizing a top cladded device through monolithic integration introduces a dilemma between mode-MO interaction (thin seedlayers are better) and quality of the MO material (thick seedlayers are best). From the results discussed so far it is evident that an industry compatible solution can be realized, if seed layer free garnets could be obtained on Si. Fortunately, the family of terbium iron garnets or TIGs do not require a seed layer for growth on Si substrates or SOI platforms. Cerium doped TIG (Ce:TIG) and bismuth doped TIG (Bi:TIG) can be grown via reactive RF magnetron co-sputtering followed by an *ex-situ* RTA to crystallize the as deposited amorphous thin films [39]. It has been demonstrated that Ce:TIG grown on different substrates like Si, quartz, MgO, and YSZ can crystallize in the desired garnet phase without a seed layer, evident from the X-ray diffraction (XRD) spectra in Fig. 6. Initial free-space optical measurements at $1.55\mu m$ resulted in a FR of $-2600°/cm$ for Ce:TIG grown on Si and further optimization of the dopant concentration and annealing temperature increased FR to $-3200°/cm$ (the highest reported to date for a seed-layer free iron garnet) [16, 39].

## 3. Device designs for NRPS and NRMC isolators

Integration of garnets on SOI platforms through monolithic techniques was deemed non-viable for a very long time due to garnet-silicon incompatibility issues as explained in the previous section. The first steps in realizing isolator devices with Si core waveguides focused on hybrid integration techniques like wafer bonding [40, 41]. In wafer bonding, epitaxial pure phase single crystal Ce:YIG is grown on lattice matched GGG substrate using vacuum deposition technique and mechanically bonded as a cladding in the region of magneto-optical operation. Isolators based on the Mach-Zehnder interferometer (MZI) design that operate under the principle of NRPS are utilized as shown in Fig. 7(a). In an MZI structure, the transverse magnetic field applied perpendicular to the waveguide arms induces a phase change of $\phi_+$ and $\phi_-$ in the left and right arms. The phase difference between the two arms can be adjusted using reciprocal phase shifters (RPS) so that the light propagating in the forward direction interferes constructively

Optical Materials EXPRESS

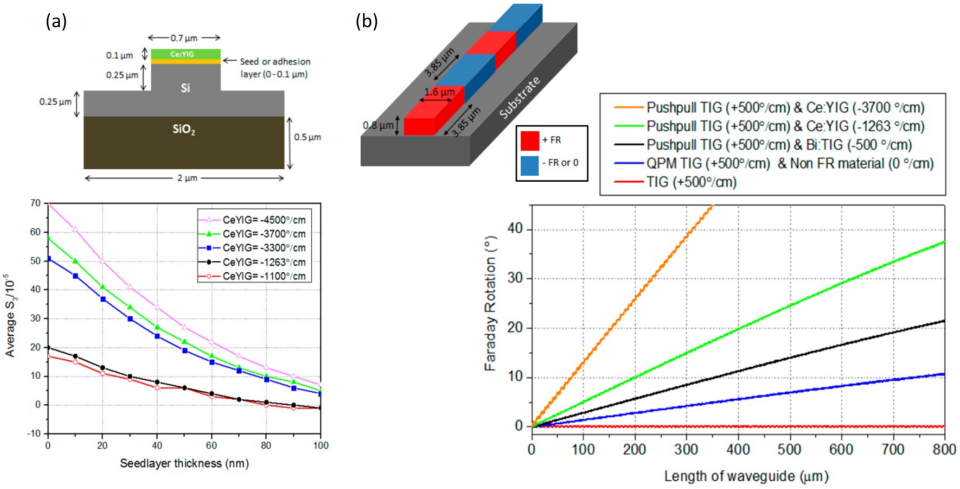


Fig. 5. (a) Finite difference time domain (FDTD) simulation to analyze the effect of seed layer thickness on the average $S_3$ Stokes parameter for TE-modes in SOI waveguides with garnet cladding. The cross sectional schematic is a reference to the structure simulated. (b) FDTD simulation of garnet core push-pull isolator device with alternate segments of $+FR$ and $FR$. The FR vs length of the waveguide data shows the 45° rotation can be achieved at lengths of $360\mu m$. Reprinted with permission from [38]. Copyright 2018 American Chemical Society.

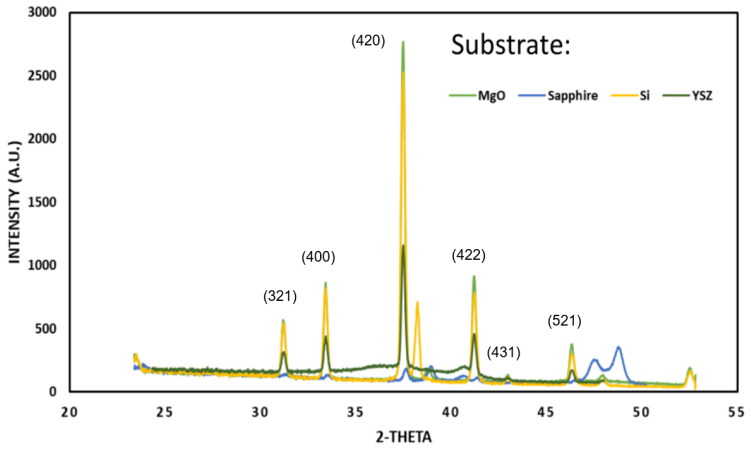


Fig. 6. XRD spectra of Ce:TIG grown on non-garnet substrates without a seed layer. The characteristic garnet peaks indicate the crystallization in the desired phase [16].

Optical Materials EXPRESS

and destructively interferes in the reverse direction, blocking the reflections. Such devices have successfully demonstrated ≥30 dB isolation ratios [40], 20 dB isolation bandwidth and low insertion loss with operation in both TM and TE modes [42]. Furthermore this hybrid integration technique has facilitated the development of ring resonator based isolators and circulators with an isolation ratio of 19.5 dB and 22 dB respectively [20, 43]. Despite the success of wafer bonding, this hybrid integration technique lacks the scalability that monolithic integration offers. Moreover, one has to note that NRPS based devices discussed in the literature so far are confined to TM-mode and TE-mode operability is achieved at the cost of larger device footprint or ancillary components for TE-TM conversion [44]. In light of several of these short comings that are crucial to a device's industry acceptance, NRMC or Faraday rotation based device's are proposed as an acceptable alternative.

As mentioned in the introduction, non-reciprocal polarization mode conversion (NRMC) is the waveguide equivalent to Faraday rotation. In this technique, the MO material is directly deposited using a vacuum deposition technique like sputtering on the Si core waveguide [45]. However, the mismatch in the waveguide dimensions causes a difference in the propagation constant between the TE and TM modes making the waveguide birefringent. It should be also be noted that Faraday rotation is a coherent form of mode conversion that is phase dependent. If there is a mismatch in the modal phase velocities, the extent of flow of energy between the two modes is restricted. This mismatch results in a periodic behavior where the phase difference of $2\pi$ is accumulated over the corresponding beat length as shown in Fig. 7(b). However, the phase mismatch can be overcome by quasi-phase matching (QPM) where the cladding is spatially modulated into alternate segments of MO and non-MO materials to ensure a monotonic flow of energy between the two modes [24]. In the presence of the alternate segments of garnet and non-garnet material, the light experiences FR during the positive cycle of the mode and does not undergo any rotation during its negative cycle. The segments are matched to the beat lengths so that the accumulated phase difference is $2\pi$. A graphic representation of a QPM segmented cladding is shown in Fig. 7(c).

In comparison to the MZI and ring resonator isolators based on NRPS, the NRMC device can operate in the TE-mode with the help of a half reciprocal polarization converter (H-RPC), as shown in Fig.7(c). The different polarization states of the light during its forward and backward propagation can be visualized with the Stokes parameter illustrated on the surface of a Poincaré sphere (Fig. 8(a)) [46]. The "equator" of the sphere corresponds to linear polarization and the "poles" represent circular polarization states. The light emerging from the source is TE which undergoes a conversion from TE to TE = TM (+45°) in the waveguide due to the MO effect which is represented by the solid line along the equator. At the output of the waveguide, the light is converted back to TE at the H-RPC denoted by the forward dashed line. In the reverse direction, the polarization state of the reflected light changes from TE to TE = TM (+45°) at the H-RPC (backward dashed line) and to TM (solid line along the equator) in the waveguide due to NRMC. Therefore, the reflected light is orthogonal to the TE mode of the laser.

The device was fabricated using lithography by periodically lifting off segments of the top garnet cladding, deposited using sputtering. The waveguide and the garnet cladding were then coated with $Si_xN_y$ for index matching to produce segment lengths corresponding to the beat lengths. The different garnet materials used in this device are Ce:YIG (80 nm) with a YIG seed layer (45 nm) and Bi:TIG (80 nm) without a seed layer. The isolation measurements were carried out using the equivalent technique of reversing the longitudinal magnetic field. First, the degree of orthogonality of the forward and backward propagation outputs we measured and plotted as the Stokes parameters. Then, isolation ratio was calculated with the respective transmissions using Malus's law.

$$Isolation\ ratio\ (dB) = 20log_{10}\left|\cos\tfrac{\theta}{2}\right| = 10log_{10}\frac{1}{2}(1 + S_+ \cdot S_-) \tag{3}$$

Optical Materials EXPRESS

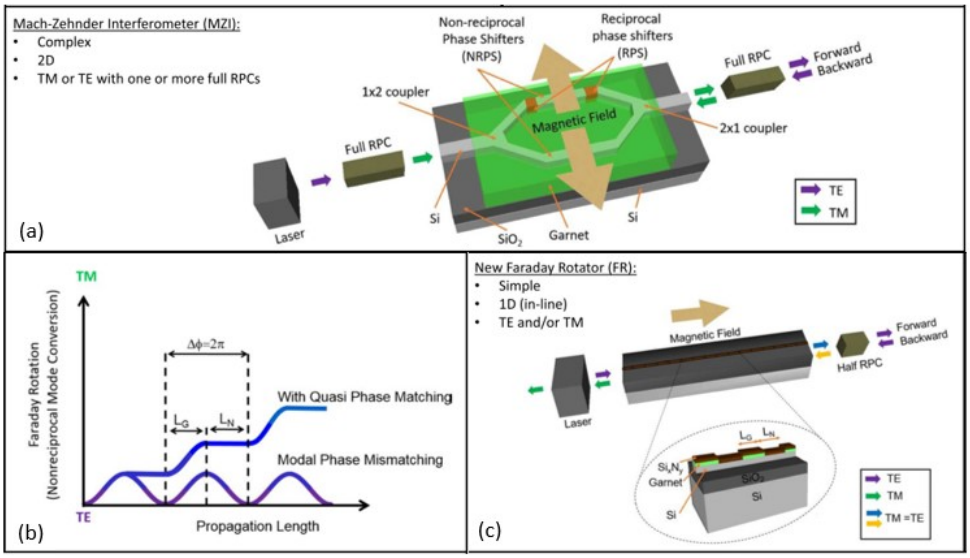


Fig. 7. Schematic representation of isolators based on NRMC (Faraday rotation) and NRPS (MZI) designs. (a) TE-mode MZI device with two full RPC and bi-directional field with hybrid integration of garnet cladding. (b) Effects of phase velocity mismatch is reflected periodically for a $2\pi$ period and it is overcome by QPM. (c) Faraday rotation waveguide isolator with a quasi-phase matched segmented garnet cladding. Reproduced from [23] under the Creative Commons license.

For a 500 nm SOI (Si core: 500 nm x 900 nm) with Ce:YIG/YIG cladding, the maximum observed Stokes vector angle was $0.74\pi$ for a 4.1 mm long device, resulting in an isolation ratio of -8 dB. The best result was produced by the seed-layer free Bi:TIG cladding in a 340 nm SOI (Si core: 340 nm x 900 nm). The maximum observed Stokes vector angle was $0.83\pi$ for a 3.4 mm long device, giving an isolation ratio of -11 dB as shown in Fig. 8(b). This is the first ever report of TE-mode Faraday rotation based isolator, and it is comparable in performance to the initial TM-mode designs [23].

## 4. Summary

This review has highlighted the steps taken in materials research of rare-earth iron garnets (YIG) essential to optical isolators in PICs with an aim to achieve monolithically integrated devices on SOI platforms. The material focus elaborated on the growth parameters for garnets and demonstrated overwhelming evidence in support of sputtering as a foundry friendly technique for depositing garnets as claddings for waveguides. It was seen that patterning of garnet eliminated the formation of cracks upon annealing and doping with cerium or bismuth increased Faraday rotation. However, a seed-layer of undoped YIG was needed to grow doped garnets and their optical properties, thermal budget requirements, fabrication complexities were analyzed using a variety of experimental and simulation techniques. As an alternative, seed layer free garnets (TIG, Ce:TIG and Bi:TIG) were proposed to overcome the limitations posed by Ce:YIG and Bi:YIG, thereby making single step deposition of MO material feasible. On the devices front, the extensive research carried out in the area of NRPS isolators was reviewed whilst highlighting the tremendous progress made in obtaining very high isolation ratios and low insertion loss over a large bandwidth. Finally, it is worth pointing out that NRMC paved way for first ever TE-mode isolator achieved via monolithic integration of the seed-layer free MO material and will lay down

Optical Materials EXPRESS

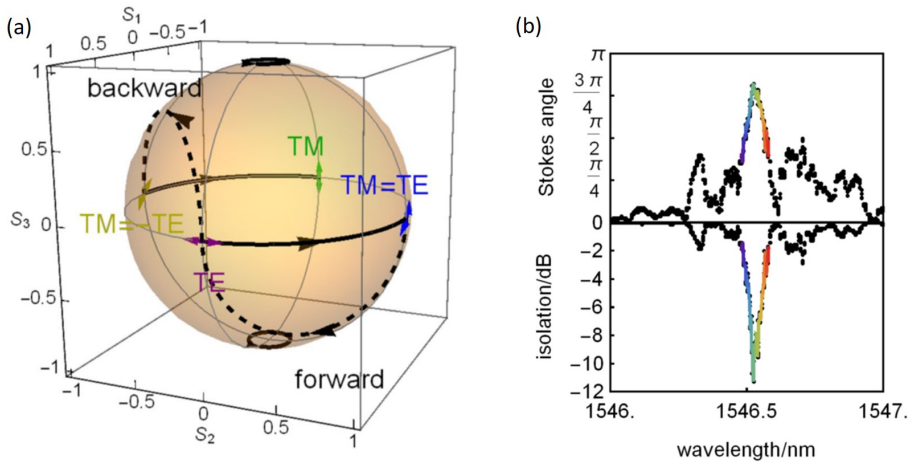


Fig. 8. (a) Poincaré sphere illustrating the change in the polarization state of the light as it propagates through the isolator. The solid lines correspond to non-reciprocal Faraday rotation and the dashed lines to the half reciprocal phase conversion. (b) Optical measurements for 340 nm Si core SOI device with Bi:TIG cladding having a maximum Stokes angle of $0.83\pi$ and an isolation of -11 dB. Reproduced from [23] under the Creative Commons license.

the framework for future integrated optical isolators.

## Acknowledgments

The authors would like to acknowledge Dr. David C. Hutchings, Dr. Cui Zhang, Dr. Sang-Yeob Sung, Dr. Andrew D. Block, Dr. Prabesh Dulal and Thomas E. Gage for their contributions to the research works highlighted in this article. Parts of this work were carried out in the Characterization Facility and the Minnesota Nano Center, University of Minnesota, which receives partial support from NSF through the MRSEC and NNCI programs respectively.

## Disclosures

The authors declare that there are no conflicts of interest related to this article.

## References

1. R. Soref, "The Past, Present, and Future of Silicon Photonics," IEEE J. Sel. Top. Quantum Electron. **12**, 1678–1687 (2006).
2. J. Leuthold, C. Koos, and W. Freude, "Nonlinear silicon photonics," Nat. Photonics **4**, 535–544 (2010).
3. R. G. Beausoleil, P. J. Kuekes, G. S. Snider, S. Y. Wang, and R. S. Williams, "Nanoelectronic and nanophotonic interconnect," Proc. IEEE **96**, 230–247 (2008).
4. J. D. Meindl, "Beyond Moore's Law: The interconnect era," Comput. Sci. & Eng. **5**, 20–24 (2003).
5. R. Nagarajan, C. H. Joyner, R. P. Schneider, J. S. Bostak, T. Butrie, A. G. Dentai, V. G. Dominic *et al.*, "Van Leeuwen, J. Webjorn, M. Ziari, D. Perkins, J. Singh, S. G. Grubb, M. S. Reffle, D. G. Mehuys, F. A. Kish, and D. F. Welch, "Large-scale photonic integrated circuits," IEEE J. Sel. Top. Quantum Electron. **11**, 50–65 (2005).
6. A. C. Nilsson, C. H. Joyner, D. F. Welch, D. D. Perkins, F. A. Kish, M. L. Mitchell, and R. Nagarajan, "The realization of large-scale photonic integrated circuits and the associated impact on fiber-optic communication systems," J. Light. Tech. **24**, 4674–4683 (2006).
7. D. Thomson, A. Zilkie, J. E. Bowers, T. Komljenovic, G. T. Reed, L. Vivien, D. Marris-Morini, E. Cassan, L. Virot, J.-M. Fédéli, J.-M. Hartmann, J. H. Schmid, D.-X. Xu, F. Boeuf, P. O'Brien, G. Z. Mashanovich, and M. Nedeljkovic, "Roadmap on silicon photonics," J. Opt. **18**, 073003 (2016).
8. M. Shirasaki and K. Asama, "Compact optical isolator for fibers using birefringent wedges," Appl. Opt. **21**, 4296–4299 (1982).

Optical Materials EXPRESS


9. D. Jalas, A. Petrov, M. Eich, W. Freude, S. Fan, Z. Yu, R. Baets, M. Popović, A. Melloni, J. D. Joannopoulos, M. Vanwolleghem, C. R. Doerr, and H. Renner, "What is – and what is not – an optical isolator," Nat. Photonics **7**, 579–582 (2013).
10. B. J. H. Stadler and T. Mizumoto, "Integrated magneto-optical materials and isolators: A review," IEEE Photonics J. **6**, 1–15 (2014).
11. B. J. H. Stadler and D. C. Hutchings, "Sputter-deposited magneto-optical garnet for all-mode (transverse electric/transverse magnetic) Faraday rotators," MRS Bull. **43**, 430–435 (2018).
12. J. F. Dillon, Jr, "Origin and Uses of the Faraday Rotation in Magnetic Crystals," J. Appl. Phys. **39**, 922–929 (1968).
13. V. Fratello and R. Wolfe, *Epitaxial Garnet Films for Nonreciprocal Magneto-Optic Devices in Handbook of Thin Films* (SPIE Press, 2000).
14. T. Tepper, F. Ilievski, C. A. Ross, T. R. Zaman, R. J. Ram, S. Y. Sung, and B. J. H. Stadler, "Magneto-optical properties of iron oxide films," J. Appl. Phys. **93**, 6948 (2003).
15. M. C. Onbasli, L. Beran, M. Zahradník, M. Kučera, R. Antoš, J. Mistrík, G. F. Dionne, M. Veis, and C. A. Ross, "Optical and magneto-optical behavior of Cerium Yttrium Iron Garnet thin films at wavelengths of 200-1770 nm," Sci. Reports **6**, 23640 (2016).
16. K. Srinivasan, T. E. Gage, and B. J. H. Stadler, "Seed-Layer Free Cerium-Doped Terbium Iron Garnet on Non-Garnet Substrates for Photonic Isolators," in *Conference on Lasers and Electro-Optics,* (Optical Society of America, San Jose, California, 2018), OSA Technical Digest (online), p. SW4I.5.
17. M. Takenaka and Y. Nakano, "Proposal of a novel semiconductor optical waveguide isolator," in *Conference Proceedings. Eleventh International Conference on Indium Phosphide and Related Materials* (IEEE, 1999), pp. 289–292.
18. Z. Yu and S. Fan, "Complete optical isolation created by indirect interband photonic transitions," Nat. Photonics **3**, 91–94 (2009).
19. S. Ghosh, S. Keyvaninia, Y. Shoji, W. Van Roy, T. Mizumoto, G. Roelkens, and R. G. Baets, "Compact Mach-Zehnder interferometer Ce:YIG/SOI optical isolators," IEEE Photonics Technol. Lett. **24**, 1653–1656 (2012).
20. L. Bi, J. Hu, P. Jiang, D. H. Kim, G. F. Dionne, L. C. Kimerling, and C. A. Ross, "On-chip optical isolation in monolithically integrated non-reciprocal optical resonators," Nat. Photonics **5**, 758–762 (2011).
21. H. Shimizu and Y. Nakano, "Fabrication and Characterization of an InGaAsp/InP Active Waveguide Optical Isolator With 14.7 dB/mm TE Mode Nonreciprocal Attenuation," J. Light. Tech. **24**, 38 (2006).
22. P. Pintus, F. Di Pasquale, and J. E. Bowers, "Design of transverse electric ring isolators for ultra-low-loss Si3N4 waveguides based on the finite element method," Opt. Lett. **36**, 4599–4601 (2011).
23. C. Zhang, P. Dulal, B. J. H. Stadler, and D. C. Hutchings, "Monolithically-Integrated TE-mode 1D Silicon-on-Insulator Isolators using Seedlayer-Free Garnet," Sci. Reports **7**, 5820 (2017).
24. D. C. Hutchings, B. M. Holmes, C. Zhang, P. Dulal, A. D. Block, S. Y. Sung, N. C. A. Seaton, and B. J. H. Stadler, "Quasi-phase-matched Faraday rotation in semiconductor waveguides with a magnetooptic cladding for monolithically integrated optical isolators," IEEE Photonics J. **5**, 6602512 (2013).
25. T. Aichele, A. Lorenz, R. Hergt, and P. Görnert, "Garnet layers prepared by liquid phase epitaxy for microwave and magneto-optical applications – a review," Cryst. Res. Technol. **38**, 575–587 (2003).
26. B. Stadler, K. Vaccaro, P. Yip, J. Lorenzo, Y. Li, and M. Cherif, "Integration of Magneto-Optical Garnet Films by Metal – Organic," Chem. Vap. Deposition **38**, 1564–1567 (2002).
27. S. Y. Sung, X. Qi, and B. J. H. Stadler, "Integrating yttrium iron garnet onto nongarnet substrates with faster deposition rates and high reliability," Appl. Phys. Lett. **87**, 1–3 (2005).
28. S.-Y. Sung, A. Sharma, A. Block, K. Keuhn, and B. J. H. Stadler, "Magneto-optical garnet waveguides on semiconductor platforms: Magnetics, mechanics, and photonics," J. Appl. Phys. **109**, 07B738 (2011).
29. Y. Shoji and T. Mizumoto, "Wideband design of nonreciprocal phase shift magneto-optical isolators using phase adjustment in Mach-Zehnder interferometers," Appl. Opt. **45**, 7144–7150 (2006).
30. M. C. Onbasli, T. Goto, X. Sun, N. Huynh, and C. A. Ross, "Integration of bulk-quality thin film magneto-optical cerium-doped yttrium iron garnet on silicon nitride photonic substrates," Opt. Express **22**, 25183–25192 (2014).
31. V. J. Fratello, S. J. Licht, and C. D. Brandle, "Innovative improvements in bismuth-doped rare-earth iron garnet Faraday rotators," IEEE Transactions on Magn. **32**, 4102–4107 (1996).
32. L. Bi, J. Hu, G. F. Dionne, L. Kimerling, and C. A. Ross, "Monolithic integration of chalcogenide glass/iron garnet waveguides and resonators for on-chip nonreciprocal photonic devices," SPIE **7941**, 794105 (2011).
33. T. Goto, M. C. Onbaşlı, and C. A. Ross, "Magneto-optical properties of cerium substituted yttrium iron garnet films with reduced thermal budget for monolithic photonic integrated circuits," Opt. Express **20**, 28507–28517 (2012).
34. A. D. Block, P. Dulal, B. J. H. Stadler, and N. C. A. Seaton, "Growth Parameters of Fully Crystallized YIG, Bi:YIG, and Ce:YIG Films With High Faraday Rotations," IEEE Photonics J. **6**, 1–8 (2014).
35. S. Ghosh, S. Keyvavinia, W. Van Roy, T. Mizumoto, G. Roelkens, and R. Baets, "Ce:YIG/Silicon-on-Insulator waveguide optical isolator realized by adhesive bonding," Opt. Express **20**, 1839–1848 (2012).
36. X. Y. Sun, Q. Du, T. Goto, M. C. Onbasli, D. H. Kim, N. M. Aimon, J. Hu, and C. A. Ross, "Single-Step Deposition of Cerium-Substituted Yttrium Iron Garnet for Monolithic On-Chip Optical Isolation," ACS Photonics **7**, 856–863 (2015).
37. T. E. Gage, P. Dulal, P. A. Solheid, D. J. Flannigan, T. E. Gage, P. Dulal, P. A. Solheid, and D. J. Flannigan, "Si-integrated ultrathin films of phase-pure Y 3 Fe 5 O 12 (YIG) via novel two-step rapid thermal anneal," Mater. Res.

Optical Materials EXPRESS

Lett. **0**, 1–7 (2017).
38. P. Dulal, A. D. Block, T. E. Gage, H. A. Haldren, S. Y. Sung, D. C. Hutchings, and B. J. H. Stadler, "Optimized Magneto-optical Isolator Designs Inspired by Seedlayer-Free Terbium Iron Garnets with Opposite Chirality," ACS Photonics **3**, 1818–1825 (2016).
39. P. Dulal, T. E. Gage, A. D. Block, E. Cofell, D. C. Hutchings, and B. J. H. Stadler, "Sputter-deposited seedlayer-free cerium-doped terbium iron garnets for SOI waveguide isolators," in *2016 IEEE Photonics Conference (IPC)* (IEEE, 2016).
40. Y. Shoji, K. Miura, and T. Mizumoto, "Optical nonreciprocal devices based on magneto-optical phase shift in silicon photonics," J. Opt. **18**, 13001 (2016).
41. D. Huang, P. Pintus, C. Zhang, P. Morton, Y. Shoji, T. Mizumoto, and J. E. Bowers, "Dynamically reconfigurable integrated optical circulators," Optica **4**, 23 (2017).
42. D. Huang, P. Pintus, C. Zhang, Y. Shoji, T. Mizumoto, and J. E. Bowers, "Electrically driven and thermally tunable integrated optical isolators for silicon photonics," IEEE J. Sel. Top. Quantum Electron. **22**, 271–278 (2016).
43. S. Ghosh, S. Keyvaninia, W. Van Roy, T. Mizumoto, G. Roelkens, and R. Baets, "Adhesively bonded Ce:YIG/SOI integrated optical circulator," Opt. Lett. **38**, 965–967 (2013).
44. S. Ghosh, S. Keyvaninia, Y. Shirato, T. Mizumoto, G. Roelkens, and R. Baets, "Optical isolator for TE polarized light realized by adhesive bonding of Ce:YIG on silicon-on-insulator waveguide circuits," IEEE Photonics J. **5**, 6601108 (2013).
45. D. C. Hutchings, C. Zhang, B. M. Holmes, P. Dulal, A. D. Block, and B. J. H. Stadler, "Faraday polarisation mode conversion in semiconductor waveguides incorporating periodic garnet claddings," Proc. SPIE **9750**, 97500V (2016).
46. D. C. Hutchings and B. M. Holmes, "A waveguide polarization toolset design based on mode beating," IEEE Photonics J. **3**, 450–461 (2011).